A Compressed Sensing-Based Imaging System

Yuri Álvarez-López[1], Yolanda Rodríguez-Vaqueiro[2], Borja González-Valdés[2], José Ángel Martínez-Lorenzo[2], Fernando Las-Heras[1], Carey M. Rappaport[2]

[1] Área de Teoría de la Señal y Comunicaciones. Universidad de Oviedo. Gijón (Asturias). Spain.
Email: yalopez@tsc.uniovi.es, flasheras@tsc.uniovi.es.

[2] The Gordon CenSSIS / ALERT Center of Excellence. Northeastern University. Boston (MA). United States.
Email: rodriguezvaqueiro.y@husky.neu.edu, bgonzale@ece.neu.edu, jmartine@ece.neu.edu, rappaport@coe.neu.edu

***Abstract*—Generating high resolution images is one of the most important capabilities of imaging systems for security applications. To achieve this goal, electrically large apertures are required, thus involving a large number of measurement samples or receivers, which leads to long acquisition times. Compressed Sensing techniques are one way to reduce the number of samples required for accurate image reconstruction. This contribution describes a multistatic millimeter wave radar imaging system which has been improved using Compressed Sensing, simplifying the imaging system design and fabrication. Performance of the system is validated by means of simulation-based examples as well as by experimental measurements.**

***Index Terms*—Millimeter waves, Imaging systems, Compressed Sensing.**

I. INTRODUCTION

In the area of homeland security, there is an increasing demand for methods to improve the efficiency of the personnel screening for concealed objects and contraband detection at security checkpoints [1-6]. Human body imaging is an effective way of identifying dangerous objects attached to the body under clothing. Terahertz wave sensing [4,5] and X-ray backscatter [5] provide good resolution, but the former is based on expensive, cutting-edge technology and its speed and accuracy depend on precise mechanical scanning, while the X-ray systems make use of ionizing radiation, which is less attractive to the airline travelers.

Millimeter-wave imaging radar systems [1-3] not only provide high-resolution imaging but also balance the trade-off between accuracy and cost. With mm-wave radar, the object of interest is first illuminated by millimeter waves and then the scattered field is measured and processed in order to reconstruct the surface (or volume) of the object. The image resolution is determined by the radar center frequency, its bandwidth, and its aperture size.

A novel millimeter wave imaging system was presented in previous works [2,3]. System layout is depicted in Fig. 1: the human body is illuminated by an incident millimeter-wave generated by a novel Blade Beam elliptical-parabolic reflector antenna. This antenna produces a narrow beam in elevation (z axis) while illuminating the body with constant amplitude in azimuth [7]. This illumination allows thin slices (~ 2-3 cm thickness) of the body to be processed independently. The electric field scattered by the illuminated section is captured by two arrays of millimeter wave antenna elements placed on a 90º arc above and below the transmitting reflector. A Synthetic Aperture Radar (SAR)-based imaging algorithm [8] is used to recover the reflectivity values on slices placed parallel to XY plane illuminated by the Blade Beam transmitting antenna. The transmitting antenna and the receiving antenna arrays are translated vertically, and the two-dimensional retrieved images are stacked to form a full body surface reconstruction [2,3]. This approach simplifies the three-dimensional reconstruction problem into a combination of multiple 2D problems allowing the reduction of computational cost and processing time of the full 3D inversion problem, an essential requirement for practical security screening systems.

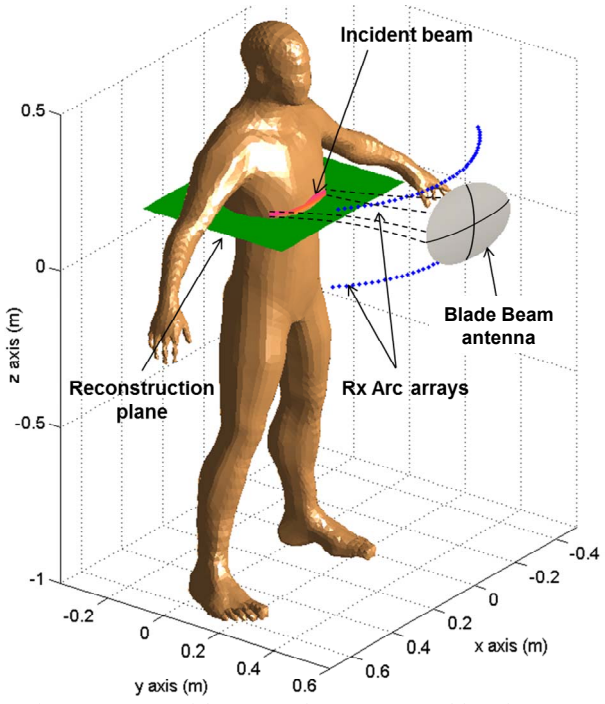

Fig. 1. Geometry of the proposed mm-wave portal-based system.

One of the remaining limitations is the number of required receivers. According to the minimum sampling rate criterion [9], for the system proposed in [2,3] (f = 60–66 GHz, human

This work is supported by CenSSIS, the Gordon Center for Subsurface Sensing and Imaging Systems NSF ERC Program (Award number EEC-9986821); by the Science and Technology Directorate, U.S. Department of Homeland Security under the Award Number "2008-ST-061-ED0001"; by the "Ministerio de Economía y Competitividad" of Spain/FEDER under projects CONSOLIDER-INGENIO CSD2008-00068 (TERASENSE), and TEC2011-24492/TEC (iSCAT).

body having a maximum cross-range size of ~40 cm) with SAR imaging, the minimum number of receivers on each arc is about 150.

Reducing the number of receivers and thereby the cost, complexity and measurement time without compromising the quality of the reconstructed image is the purpose of this research. To achieve this, Compressed Sensing (CS) techniques, which have been successfully applied in several imaging problems (CS-SAR) [10-13], are proposed. Usually, CS-SAR images are generated with as few as 25-30% of the samples required by standard SAR imaging.

II. Compressed Sensing Technique

Compressed Sensing (CS) [14-16] states that sparse signals can be recovered using far fewer samples or measurements than that required by the Nyquist sampling criterion. A discrete signal vector $y \in C^N$ can be represented in terms of an orthonormal basis $\Psi \in C^{N\times N}$ as (1):

$$y = \Psi \alpha , \tag{1}$$

$\alpha \in C^N$ represents the coefficient vector. The signal y is K-sparse if it is a linear combination of only K basis vectors; that is, α only has K non-zero coefficients, with $K << N$.

The *subsampled* signal y_s, is acquired by linear projection $y_s = \Phi y$. $\Phi \in C^{M\times N}$ is a binary matrix: with ones corresponding to the receiver locations, and zeroes corresponding to the discarded positions, both sets randomly selected. M denotes the number of measurements needed, which satisfies $M << N$.

$$y_s = \Phi y = \Phi\Psi\alpha = \Theta\alpha , \tag{2}$$

where Θ is an $M \times N$ matrix. Although (2) is underdetermined, it has been shown that it is very likely to recover $y = \Psi\alpha$ exactly, provided that α is a sparse signal and that matrix Θ obeys a Restricted Isometry Property (RIP), which is satisfied if Ψ and Φ are incoherent.

As stated in [14], any random matrix Φ is likely incoherent with the orthonormal basis Ψ. Numerical evaluation of the coherence (represented by $\mu(\Theta^*, \Theta)$) of $\Theta = \Psi\Phi$, can be assessed as indicated in Eq. (3) of [14]. When the samples are corrupted with noise, as occurs in real problems, the minimization problem to be solved is:

$$\min_{\alpha\in R^N} \|\alpha\|_1 \quad subject\ to \quad \|y_s - \Theta\alpha\|_2 < \varepsilon , \tag{3}$$

A cross-validation technique, as described in [15], is used to determine the value of the regularization parameter ε. The Nesterov algorithm [16], provided as a Matlab® toolbox, is used to minimize Eq. (3).

An additional advantage of CS-SAR imaging derived from the aforementioned mm-wave portal-based scanner is that the number of non-zero elements can be estimated using *a-priori* information. Assuming that the slice where the CS-SAR image is recovered is discretized into $(N)^{1/2}\times(N)^{1/2}$ pixels (N is the number of elements of vector y) then it is possible to estimate that the number of non-zero reflectivity elements will be $K \sim (N)^{1/2}$ assuming one-pixel range thickness of the slice and that the recovered profile occupies the entire cross-range dimension. Moreover, it has been observed that the sparse signal can be accurately recovered with a number of samples of $M \sim 4K$ [17]. Thus the expected number of non-zero reflectivity pixels of α, K, is related to the minimum number of samples (y_s vector) M to be used for the reconstruction.

III. CS Human Body 3D Profile Reconstruction

This section presents an application example of the CS techniques for the proposed personnel screening system. The object-under-test consists of a realistic model of the human body torso with two attached objects [2-3], as depicted in Fig. 2.

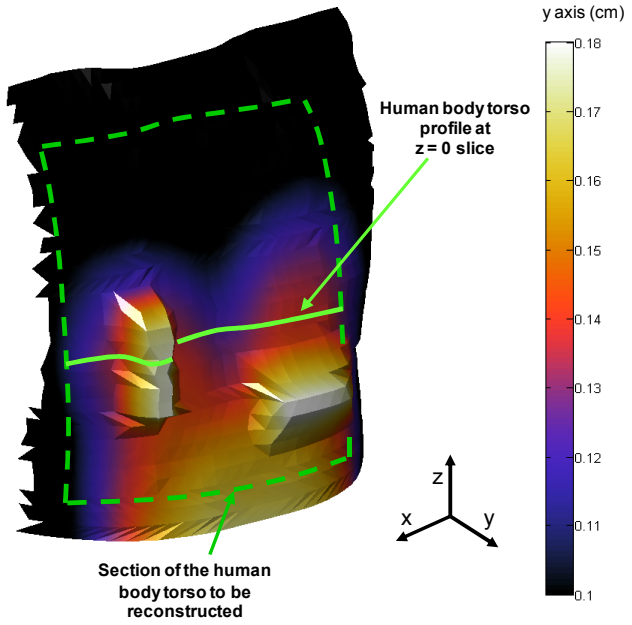

Fig. 2. Object-under-test: portion of the human body torso with two attached objects. The dashed green line represents the portion of the torso to be recovered. Solid green line indicates torso profile for the z = 0 m slice.

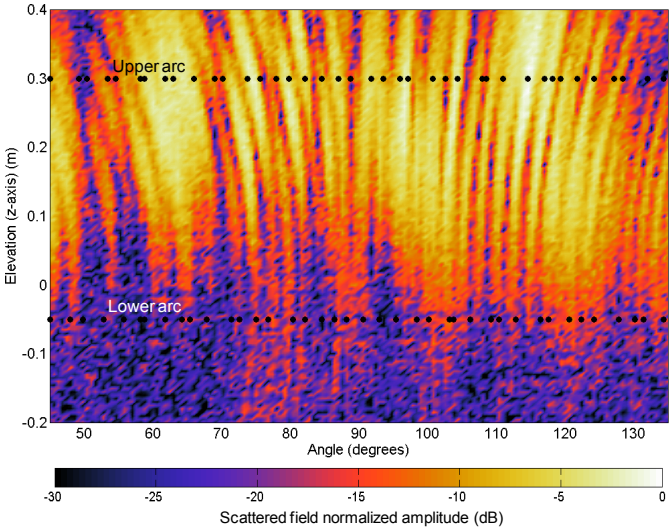

Fig. 3. Field scattered by the human body torso at f = 60 GHz when the beam is pointing at elevation z = 0 m. Two arcs are used. Black dots indicate the randomly chosen receiver positions (P = 40 positions per arc).

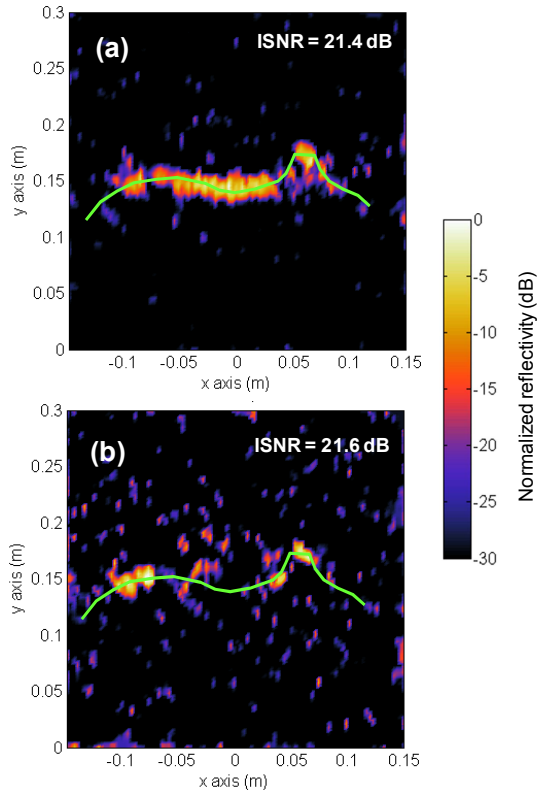

Fig. 4. CS-SAR images (normalized reflectivity, dB) recovered on the z = 0 m slice using P = 40 receiving positions. (a) Upper arc. (b) Lower arc. Green line represents the true human body torso profile at z = 0 m.

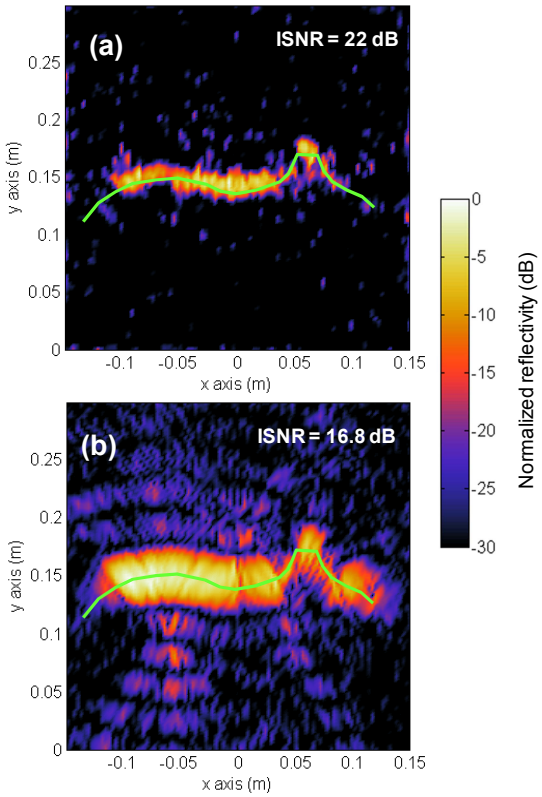

Fig. 5. (a) CS-SAR, with 40 receivers per arc image and (b) standard SAR, with 150 receivers per arc image (normalized reflectivity, dB) recovered on the z = 0 m slice combining upper and lower arc results. Green line represents the true human body torso profile at z = 0 m.

The forward problem is simulated with physical optics (PO), assuming that the human body behaves as a good conductor in the 60.6-66 GHz frequency band. This band is sampled at 600 MHz frequency steps, thus resulting in F = 10 samples in frequency. White Gaussian noise is added to the simulated scattered field for a realistic Signal-to-Noise Ratio of 30 dB.

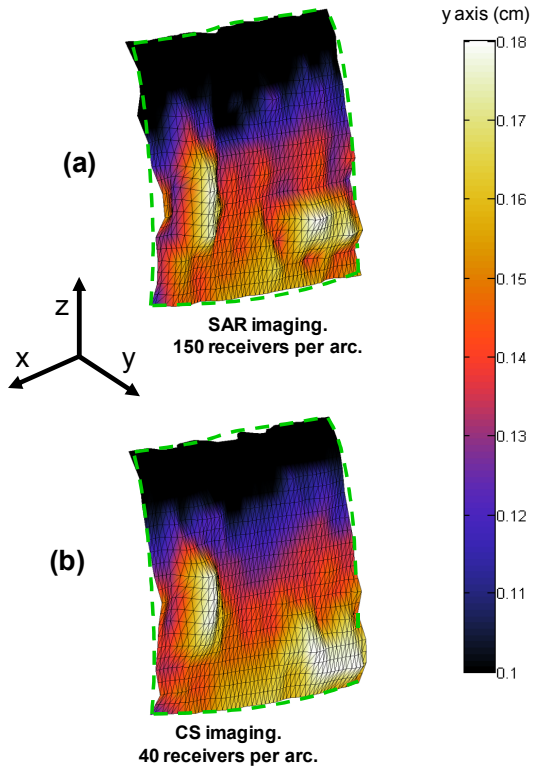

Fig. 6. Reconstructed meshes generated from the stacked 2D standard SAR images using two arcs of 150 receivers (a) and CS-SAR images using two arcs of 40 receivers (b).

First, the CS method is validated for a single slice corresponding to when the Blade Beam illuminates the torso along z = 0 m. The two 90º-arcs are placed 30 cm above and 5 cm below the reflector antenna. As mentioned in the Introduction, each arc has 150 receiving positions to avoid aliasing. The use of two arcs ensures that part of the scattered field will be collected in at least one of the two arcs, as shown in Fig. 3. The reconstruction slice at z = 0 m, is 0.3 x 0.3 m, centered at (x,y)=(0,0.15) m.

CS is applied using a subset of P random positions taken from the available 150 samples on each arc (black dots in Fig. 2). Cases for P = 32, 40, and 48 have been tested, finding that P = 40 provides acceptable results. For this number of samples, the reconstruction domain is discretized in N = 100 x 100 subdomains, to satisfy $M \sim 4K$, with $K \sim (N)^{1/2}$, and $M = F$ x P = 400 samples.

Two CS reflectivity images, one per arc, are recovered (see Fig. 4). Note that since the upper arc collects more power than the lower arc, the reconstructed image from the former (Fig 4 (a)) is closer to the true human body torso profile. Quantitative assessment of the image quality is given by the Image Signal-to-Noise Ration (ISNR) defined in Eq. (15) of

[15]. ISRN is 21.4 dB (Fig. 4 (a)) and 21.6 dB (Fig. 4 (b)) for the upper and lower arc respectively.

The two previous CS-SAR reflectivity images are combined in amplitude and phase to provide a single CS-SAR image at z = 0 m slice (Fig. 5 (a)). For comparison purposes, the standard SAR image is recovered using the entire set of 150 receivers on each arc (Fig. 5 (b)). It is clear that the CS image not only requires 60% fewer receivers but also that it can sharpen the human body profile with respect to standard SAR. This results in higher ISNR, and easier and more accurate automatic profile extraction and 3D mesh generation [2,3].

Next, CS-SAR and standard SAR reflectivity images are recovered on a set of slices ranging from z = -12 cm to z = + 10 cm, in 2 cm-steps. Reflectivity image reconstruction follows the same procedure as described for the z = 0 cm slice.

Once all the images have been retrieved on every slice, an automatic profile extraction method [2,3] is applied to create a 3D mesh of the human body torso. 3D meshes from standard SAR and CS-SAR images are plotted in Fig. 6(a) and 6(b) respectively. Both the human body torso, and the metallic objects attached to it are accurately reconstructed, as seen by comparing to the true human body torso depicted in Fig. 2. Again, it must be remarked that CS-SAR requires just 40 receivers per arc whereas standard SAR uses 150 (almost 4 times as many receivers) to produce almost the same 3D reconstructed mesh.

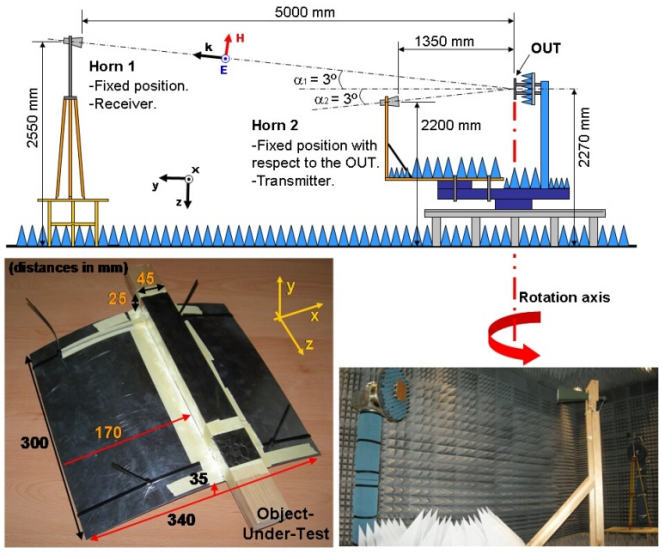

Fig. 7. Measurement setup (top). Metallic OUT, which has constant cross section along z-axis (height) (bottom left). Anechoic chamber (bottom right).

Computational cost is another key factor concerning the final implementation of a real-time portal-based mm-wave imaging system. In this sense, standard SAR processing is faster than CS-SAR, as the former can be easily implemented using forward techniques as described in [8,18]. For this example, and for every slice, standard SAR processing using 150 receivers takes 5 s, whereas CS-SAR requires 20 s with 40 samples per arc. A conventional laptop (Intel Core i5 at 2.67 GHz with 4 GB RAM) has been used for benchmarking. Despite being 4 times slower, attention must be focused on the overall calculation time for CS-SAR: 20 s times 12 slices = 240 s, far from the real-time goal. Fortunately, recent advances on Graphics Processing Units (GPUs) applied to inverse problems provide speed-up from 50x to 100x [18].

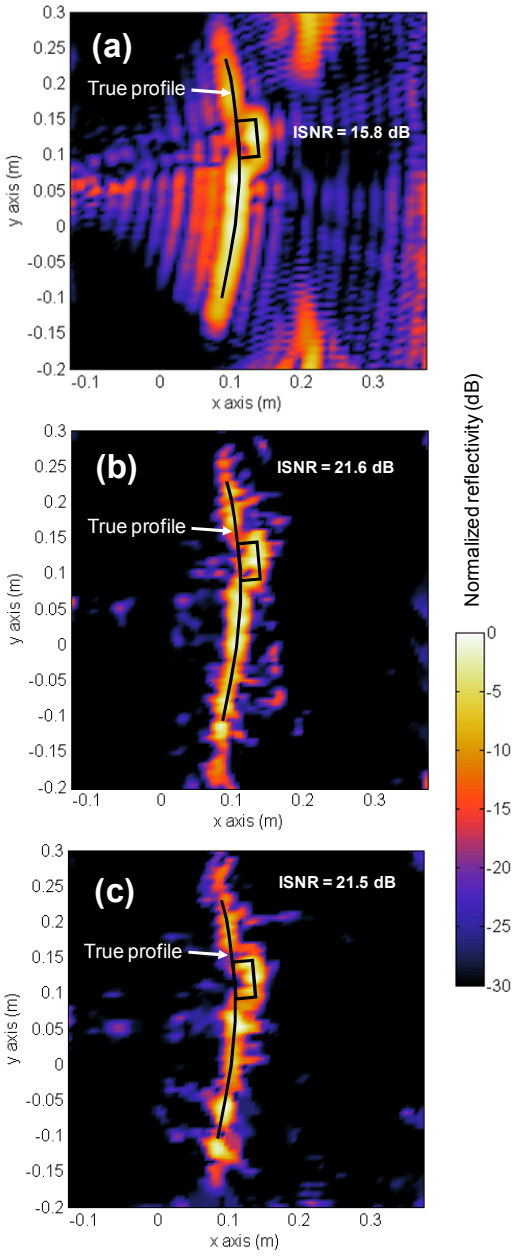

Fig. 8. (a) Standard SAR image created with 46 positions. Aliasing effects are visible along the x = 0.2 m vertical line. CS-SAR images obtained from (b) 30 and (c) 25 randomly positioned samples respectively. Solid black line represents the OUT profile.

IV. Validation with Experimental Measurements

The next step is devoted to experimental validation using measurements: for this goal, a multistatic radar setup, depicted in Fig. 7, has been mounted at the spherical range in an anechoic chamber of the University of Oviedo.

The object-under-test (OUT) is a curved metallic surface (Fig. 7, bottom left) that resembles the human body torso curvature. A 2.5 cm thick metallic object (wood prism covered with aluminum foil) is attached at the front. The frequency

ranges from 20 to 26 GHz, sampled every 500 MHz. The field scattered by the metallic target has been measured on a 90º degrees arc placed 5 m away of the object. For this configuration, the measurement setup does not allow displacement along z axis, thus allowing for 2D imaging only (profile reconstruction on the XY plane). The reconstruction domain, with size 0.5 x 0.5 m, is discretized into 80 x 80 subdomains.

First, the OUT cross-section is retrieved using standard SAR imaging. Taking into account the OUT cross-range size (34 cm), 60 samples are required along the 90º-arc to avoid aliasing [9]. Even with as few as 46 equally-spaced samples, almost aliasing-free standard SAR image can be recovered (Fig. 8 (a)).

Taking the standard SAR image as a reference, CS-SAR is tested using fewer receivers. Two different random set of positions, each having 30 and 25 samples, are chosen. CS-SAR images are depicted in Fig. 8(b) and 8(c). CS-SAR provides sharper profile reconstruction (resulting in higher ISNR), requiring as few as 25 samples, which is 51% of the information used in the almost alias-free standard SAR image (Fig. 8(a)).

Concerning calculation time, standard SAR with 46 samples takes 3 s, 5 times faster than CS-SAR (15 s with 25 samples).

V. CONCLUSION

Compressed Sensing (CS) techniques allow for a cost-effective mm-wave imaging system implementation, as accurate images can be reconstructed with fewer receivers.

Results show that CS-SAR yields an accurate 3D profile reconstruction using only 25% of the minimum number of receivers required for standard SAR imaging processing. Even for an extreme case in which the object under test can be reconstructed with standard SAR using fewer samples than Nyquist, CS-SAR requires only about half of these samples.

The main CS-SAR drawback is the computational cost: standard SAR processing is 4 to 5 times faster than CS-SAR. Thus, further research is devoted to calculation time reduction by means of GPUs.

REFERENCES

[1] D. M. Sheen, D. L. McMakin, T. E. Hall, "Three-Dimensional Millimeter-Wave Imaging for Concealed Weapon Detection," *IEEE Transactions on Microwave Theory and Techniques*, Vol. 49, No. 9, pp. 1581-1592, September 2001.

[2] Yuri Álvarez, Borja Gonzalez-Valdés, José Ángel Martínez, Fernando Las-Heras, Carey M. Rappaport, "3D Whole Body Imaging for Detecting Explosive-Related Threats, " *IEEE Transactions on Antennas And Propagation*, Vol. 60, No. 9, pp. 4453-4458, September 2012.

[3] Borja Gonzalez-Valdes, Yuri Alvarez, Jose A. Martinez, Fernando Las-Heras, Carey M. Rappaport, "On the Use of Improved Imaging Techniques for the Development of a Multistatic Three-Dimensional Millimeter-Wave Portal for Personnel Screening," *Progress In Electromagnetics Research,* PIER, Vol. 138, pp. 83-98, 2013.

[4] K. B. Cooper, R. J. Dengler, N. Llombart, B. Thomas, G. Chattopadhyay, P. H. Siegel, "THz Imaging Radar for Standoff Personnel Screening," *IEEE Transactions on Terahertz Science and Tec*hnology, Vol.1, pp.169-182, Sept. 2011.

[5] F. Friederich, W. von Spiegel, M. Bauer, F. Meng, M. Thomson, B. Lisauskas, B. Hils, V. Krozer, A. Keil, T. Löffler, R. Henneberger, A. Huhn, G. Spickermann, P. Bolívar, H. Roskos, "THz Active Imaging Systems With Real-Time Capabilities", *IEEE Transactions on Terahertz Science and Technology*, vol. 1, no. 1, pp. 183-200, 2011.

[6] R. Eilbert, S. Shuanghe, "Improved imaging for X-ray inspection systems," *IEEE Aerospace Elect Sys Mag*, Vol 20, No 3, pp 23-28, 2005.

[7] C. Rappaport, B. González-Valdés, "The Blade Beam Reflector Antenna for Stacked Nearfield Millimeter-Wave Imaging," *IEEE International Symposium on. Antennas and. Propagation*, Chicago, July 2012, pp. 1-2.

[8] Y. Alvarez, J. A. Martínez, F. Las-Heras, C. M. Rappaport, "An inverse Fast Multipole Method for geometry reconstruction using scattered field information," *IEEE Transactions on Antennas and Propagation*, Vol. 60, No. 7, pp. 3351-3360, July 2012.

[9] J. E. Hansen, "Spherical near-field antenna measurements," *IEE Electromag. Waves Series* 26. London, U.K.: Peter Peregrinus, 1988.

[10] S.-J. Wei, X.-L. Zhang, J. Shi, and G. Xiang, "Sparse Reconstruction for SAR Imaging based on Compressed Sensing," *Progress In Electromagnetics Research* PIER, Vol. 109, pp. 63-81, 2010.

[11] Vishal M. Patel, Glenn R. Easley, Dennis M. Healy, Jr., Rama Chellappa, "Compressed Sensing with Synthetic Aperture Radar Imaging," Proc. On the 16th *IEEE International Conference on Image Processing* (ICIP 2009). Cairo, Egypt, 7-10 Nov. 2009. pp. 2141-2144.

[12] Gabriel Rilling, Mike Davies, Bernard Mulgrew, "Compressed sensing based compression of SAR raw data," *Proc. On Signal Processing with Adaptive Sparse Structured Representations*, SPARS'09. April 06-09, 2009 - Saint-Malo (France). pp. 1-6.

[13] J. A. Martínez-Lorenzo, Y. Rodríguez-Vaqueiro, C. M. Rappaport, A. G. Pino, O. Rubiños, "A compressed sensing approach for detection of explosive threats at standoff distances using a Passive Array of Scatters," In *Proc. of IEEE International Conference on Homeland Security Technologies* (HST'12). Waltham, MA, November 2012.

[14] J. E. Candès, M. Wakin, "An Introduction to Compressive Sensing," *IEEE Signal Processing Mag.*, Vol. 25, No. 2, pp. 21-30, March 2008.

[15] Wenji Zhang, Moeness G. Amin, Fauzia Ahmad, Ahmad Hoorfar, and Graeme E. Smith, "Ultrawideband Impulse Radar Through-the-Wall Imaging with Compressive Sensing," *International Journal of Antennas and Propagation*, vol. 2012, Article ID 251497, 11 pages, 2012.

[16] Stephen Becker, Jérôme Bobin, Emmanuel J. Candès, "NESTA: A Fast and Accurate First-Order Method for Sparse Recovery," *SIAM Journal on Imaging Sciences*, Vol. 4, No. 1, pp. 1-39. 2011.

[17] A. Moghadam, H. Radha, "Complex Sparse Projections for Compressed Sensing," *44th Annual Conference on Information Sciences and Systems* (CISS), 2010. 17-19 March, 2010. Princeton, USA, pp. 1-6.

[18] Y. Álvarez, J. Laviada, L. Tirado, C. García, J. A. Martínez, F. Las-Heras, C. Rappaport, "Inverse Fast Multipole Method for Monostatic Imaging Applications," *IEEE Geoscience and Remote Sensing Letters*, Vol. 10, No. 5, pp. 1239-1243, September 2013.